In Situ Measurement of Magnetization Relaxation of Internalized Nanoparticles in Live Cells

Dalibor Soukup,[†] Sandhya Moise,[†] Eva Céspedes,[†,‡] Jon Dobson,[§] and Neil D. Telling*[,†]

[†]Institute for Science and Technology in Medicine, Keele University, Stoke-on-Trent, Staffordshire ST4 7QB, U.K., [‡]IMDEA NANOCIENCIA, C/Faraday, 9 Ciudad Universitaria de Cantoblanco, 28049 Madrid, Spain, and [§]J.Crayton Pruitt Family Department of Biomedical Engineering & Department of Materials Science and Engineering, University of Florida, Gainesville, Florida 32611, United States

ABSTRACT Magnetization relaxation mechanisms strongly influence how magnetic nanoparticles respond to high-frequency fields in applications such as magnetic hyperthermia. The dominant mechanism depends on the mobility of the particles, which will be affected in turn by their microenvironment. In this study AC susceptometry was used to follow the *in situ* magnetic response of model systems of blocked and superparamagnetic nanoparticles, following their cellular internalization and subsequent release by freeze–thaw lysis. The AC susceptibility signal from internalized particles in live cells showed only Néel relaxation, consistent with measurements of immobilized nanoparticle suspensions. However, Brownian relaxation was restored after cell lysis, indicating that the immobilization effect was reversible and that nanoparticle integrity was maintained in the cells. The results presented demonstrate that cellular internalization can disable Brownian relaxation, which has significant implications for designing suitable nanoparticles for intracellular hyperthermia applications. Further to this, the results highlight the possibility that particles could be released in reusable form from degrading cells following hyperthermia treatment, and subsequently reabsorbed by viable cells.

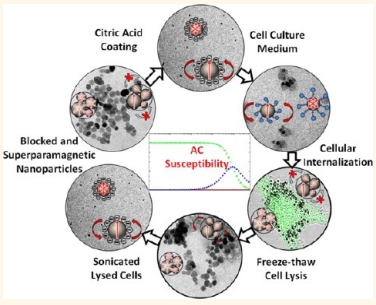

KEYWORDS: AC susceptibility · hyperthermia · magnetic nanoparticles · magnetization relaxation · cellular internalization

Magnetic nanoparticles have been widely used in biomedicine in applications such as magnetic separation, temperature induced drug delivery, cancer therapy and as contrast agents for magnetic resonance imaging (MRI).[1,2] A particularly interesting application is the use of nanoparticles for a magnetic heating (hyperthermia) based cancer treatment. Cancer cells are much more sensitive to heat shock than normal healthy cells, and when exposed to temperatures above 43–45 °C, their proliferation and metabolic activity is inhibited, which can lead to either apoptosis or necrosis.[3,4] Magnetic hyperthermia exploits the heat generated by magnetic nanoparticles when stimulated by an external high-frequency alternating magnetic field (AMF), to provide local heating to targeted cancer cells.[5,6] The transformation of electromagnetic energy into heat occurs when the frequency-dependent magnetization *versus* applied field (M-H) shows a closed loop response, such as that seen in alternating current (AC) hysteresis. The energy released per cycle of the applied field is proportional to the area of this closed loop. However, although hysteresis loss heating shows great potential for hyperthermia applications, to date it has proved a challenging task to tune the nanoparticle properties to obtain a sufficient heating effect within clinically allowed magnetic field conditions.[7,8]

When the AMF amplitude is sufficiently small, a hysteresis-like M-H loop can also be obtained because of the phase lag between the external field and the nanoparticle magnetization, caused by magnetization relaxation processes.[4,6,7,9] For particles with permanent (stable) magnetization (known as magnetically blocked particles), a Brownian mechanism of magnetization relaxation can occur due to scattering of the particles in solution, provided that the particles are free to move (Figure 1A).[10] On the other hand, superparamagnetic nanoparticles can relax purely by thermal processes: an effect known as Néel relaxation (Figure 1A) .[11] In both relaxation

* Address correspondence to n.d.telling@keele.ac.uk.

Received for review July 15, 2014 and accepted January 6, 2015.

Published online January 06, 2015
10.1021/nn503888j

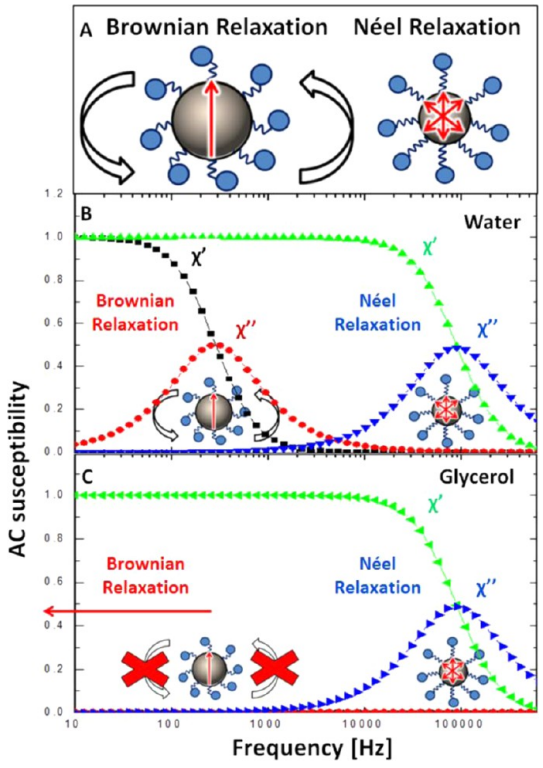

Figure 1. Schematic representation of the Brownian and Néel relaxation mechanisms of nanoparticles (A) and their corresponding AC susceptibility curves in water (B) and in glycerol (C), representing low and high viscosity dispersions, respectively. The in-phase and out-of-phase components of the complex AC susceptibility are labeled in the usual notation as χ' and χ'' respectively.

mechanisms a strong heating effect is found when the relaxation time is matched to the time period of the AMF, as this leads to the optimum phase lag and consequently the largest M-H loop area. However, reducing nanoparticle mobility can suppress the Brownian mechanism and lead to a loss of the heating effect, as seen when magnetically blocked particles are suspended in high viscosity suspensions.[10,12,13] In contrast, superparamagnetic nanoparticles can still undergo Néel relaxation and thus generate heat, even when completely immobilized.[14] To achieve significant heating effects in the latter case, precise control of magnetic nanoparticle properties such as their size and polydispersity is required.[15,16]

Perhaps the most sophisticated potential cancer therapy based on magnetic hyperthermia is the use of *intracellular heating*, which remains a relatively unexplored area.[4,13,17,18] In this case the nanoparticles are internalized and accumulate within live cells before being exposed to the AMF such that heat is generated directly inside the cells. In principle, because of the more localized nature of this form of heating,[19] much lower nanoparticle concentrations should be required in order generate apoptosis or necrosis of the cancer cells, thus minimizing systemic treatments while maximizing the probability that every cancer cell is affected. However, to date intracellular magnetic hyperthermia has proved to be challenging since insufficient heating has been generated by nanoparticles once internalized by cells.[13] Thus, the ability to probe the magnetization relaxation mechanism of these internalized nanoparticles *in situ* is essential to determine how to generate effective heating, and to assess how the nanoparticle properties can be tailored for intracellular hyperthermia applications.

The magnetization relaxation of suspensions of nanoparticles can be determined by measuring the (complex) AC magnetic susceptibility, $\tilde{\chi} = \chi' + i\chi''$.[16,20−22] The AMF frequency at which optimum phase lag occurs for a given particle type can be seen as a peak in the out-of-phase, χ'', susceptibility component (Figure 1B). For magnetically blocked particles that are free to move, the peak position reveals the Brownian relaxation time (see Figure 1A,B) and can be used to calculate the hydrodynamic size of the particles according to eq 1. When the mobility of such particles is reduced (*e.g.*, by increasing the viscosity of the suspension) the Brownian relaxation mechanism is suppressed and both the χ' and χ'' susceptibility components are lost (Figure 1C). However, the susceptibility components for superparamagnetic nanoparticles reflect the Néel relaxation, and as such are insensitive to the mobility of the particles (Figure 1B, C). In practice the Néel relaxation "peak" in χ'' is very much broadened due to polydispersity in the magnetic core sizes of the particles.[15,23,24]

Thus, AC susceptibility provides a direct method for determining the effect of the microenvironment on the magnetization relaxation of nanoparticles, and conversely, an indirect method for probing the microenvironment of the particles. However, to our knowledge, such measurements have not previously been used to assess magnetic nanoparticles in live cells. For *in vitro* and *in vivo* applications the interaction of the nanoparticles with the microenvironment cannot be neglected as it is critically important for intracellular hyperthermia. The resulting cell-particle interactions will depend on numerous parameters including the cellular microstructure, the intracellular location of internalized particles, and the particle coatings used. In particular, in order to assess if specific nanoparticles are suitable for intracellular hyperthermia, it is essential to know which relaxation mechanisms persist at each step of their lifetime cycle (from stable suspension to cellular internalization and subsequent release).

In this study a novel application of AC susceptometry, as a noninvasive method, was used to probe the *in situ* magnetization relaxation of nanoparticles in different biological environments. Model systems of both blocked and superparamagnetic nanoparticles, typical of those investigated for magnetic hyperthermia applications were studied, *i.e.*, commercially available synthetic polydisperse magnetite nanoparticles

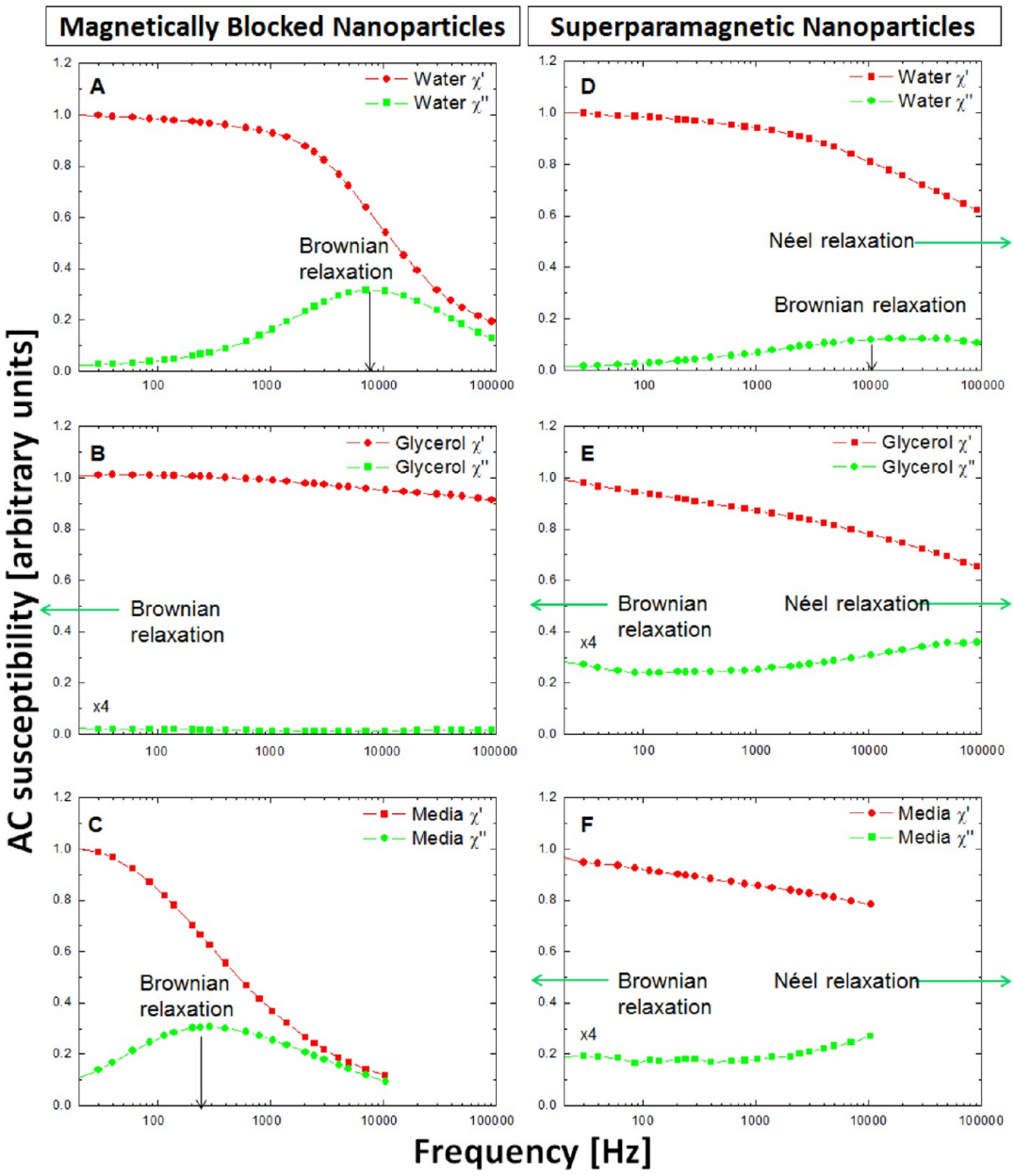

Figure 2. AC Susceptibility curves of magnetically blocked nanoparticles in water (A), in glycerol (B) and in cell culture media (C), and for superparamagnetic nanoparticles in water (D), in glycerol (E) and in cell culture media (F). χ'' signal is scaled (×4) for samples where indicated. For ease of visualization, data were normalized such that the maximum χ' values were unity in each case. For more dilute samples (C, F) the frequency range was limited to 10 kHz due to reduced sensitivity of the instrument at the higher frequencies.

consisting of mainly blocked particles (average magnetic core sizes of 23.8 ± 0.5 nm), and smaller predominantly superparamagnetic nanoparticles produced by iron reducing bacteria (average magnetic core sizes of 10.5 ± 0.4 nm).[25,26] The magnetization relaxation was probed in cell culture media, following cellular internalization in live MG-63 osteosarcoma cells, and after subsequent freeze−thaw lysis.

RESULTS AND DISCUSSION

Before evaluation of the AC susceptibility of the nanoparticles in live cells, measurements were performed on the two nanoparticle types suspended under different biologically relevant conditions. Figure 2 shows the AC susceptibility curves measured from both magnetically blocked nanoparticles (Figure 2A−C) and superparamagnetic nanoparticles (Figure 2D−F), in water (a low viscosity suspension), glycerol (a high viscosity) and cell culture media.

In water, synthetic magnetite showed a clear peak in the χ'' susceptibility component at approximately 9 kHz (Figure 2A), which corresponds to Brownian relaxation of the magnetically blocked nanoparticles. The hydrodynamic size of these particles, calculated

from eq 1 is ~46 nm which is in agreement with measurements using dynamic light scattering (DLS) (47.3 ± 2.4 nm).

In glycerol the χ'' susceptibility component disappeared (Figure 2B) because of the reduced mobility of the nanoparticles in this high viscosity suspension. The Brownian contribution to the χ'' susceptibility in this case occurs at frequencies below the measurable range. However, the χ' signal remains present in Figure 2B, in contrast to the expected result depicted in Figure 1C. In fact TEM image analysis of particle magnetic core sizes (Figure S1, Supporting Information) revealed that the synthetic magnetite sample is composed of two distinct populations of particles; the majority represented by magnetically blocked particles and a small portion (~12% by number) of superparamagnetic particles. This minority superparamagnetic population is likely to be responsible for the residual χ' susceptibility component seen in Figure 2B (see Supporting Information, Section 2).

In cell culture media (of similar viscosity to water), a peak in χ'' can be seen due to Brownian relaxation (Figure 2C), but this is shifted to a lower frequency than that found in water, corresponding to an increase in the hydrodynamic size to ~127 nm (determined by substituting the viscosity for cell culture media in eq 1). The origin of this increase could be a clustering effect that can occur following a change of microenvironment from water to media due to differences in ionic strength, or the binding of proteins from the media to the particle surfaces; an effect sometimes referred to as the protein corona.[27] Cell culture media is a complex cocktail containing charged proteins which tend to spontaneously adsorb on the largely negatively charged surface of citric acid coated nanoparticles.

As expected, results for the mainly superparamagnetic nanoparticles differed from their magnetically blocked counterpart (Figure 2D−F). In water (Figure 2D), the χ'' susceptibility contains contributions from both the Brownian and Néel relaxation mechanisms. An estimate of the hydrodynamic sizes of the superparamagnetic particles (as opposed to their magnetic core sizes) can be made by assuming an approximate Brownian maximum at ~10 kHz, giving a value of ~44 nm which is consistent with DLS measurements (45.0 ± 0.15 nm). On immobilization in glycerol (Figure 2E) the Brownian contribution is much reduced and the smaller Néel effect dominates, with a maximum χ'' occurring somewhere above the highest measured frequency (100 kHz). Unlike the magnetically blocked particles, no significant Brownian contribution is observed in media (Figure 2F). This is due to the fact that only a small proportion of nanoparticles in the superparamagnetic sample are magnetically blocked at lower frequencies, and so Brownian relaxation in this frequency region is minimal. This effect is related to the polydispersity of the magnetic core sizes.[28]

From Figure 2 it can be seen that the effect of the microenvironment on the magnetization relaxation of the nanoparticles can be effectively evaluated by AC susceptibility. An additional advantage of the technique is that the hydrodynamic particle sizes measured are inherently specific to magnetic particles, thus avoiding complications that arise in light scattering measurements from contaminants or larger protein aggregates in the suspensions.

Following this initial assessment of the magnetization relaxation of the two particle types, the nanoparticles were incubated with MG-63 osteosarcoma cells to allow cellular internalization. In a concurrent experiment the (incubation time dependent) nanoparticle uptake in the live cells was monitored using AC susceptibility (see Supporting Information, Section 3). These additional measurements confirmed that the amplitude of the AC susceptibility signal positively scaled with the internalized nanoparticle population (Figure S3). Following nanoparticle loading and AC susceptibility measurements, cell viability was evaluated using a standard live/dead staining technique. Fluorescence micrographs are shown in Figure 3A−C and confirm that the cells remained viable following susceptibility measurements, with no evidence of dead cells (stained red) found in any of the areas studied.

From bright field images (Figure 3G−I), clusters of nanoparticles appear to be localized in the peri-nuclear region of the cells. To better visualize the internalized particles, a composite confocal micrograph was obtained of vertical sections from the apex to the base of cells using fluorescence and bright field microscopy (Figure 3D−F). These measurements indicated that both nanoparticle types were readily internalized. Cellular morphology was consistently polygonal in shape and well-spread throughout the experiments, a healthy morphology further indicating that the nanoparticles did not affect cell viability.

Figure 4 shows AC susceptibility curves from magnetically blocked and superparamagnetic internalized nanoparticles measured *in situ* in the cell culture experiments. The χ'' susceptibility curve from magnetically blocked nanoparticles in cells (Figure 4A) closely resembled that of the same particles in glycerol (Figure 2B) revealing a loss in Brownian relaxation. This suggests that the particles are either immobilized, or clustered into aggregates larger than ~400 nm (the maximum hydrodynamic size that can be detected within the frequency range of the instrument). Interestingly, however, after cell lysis to release the internalized nanoparticles, Brownian relaxation was restored with a clear peak in χ'' seen at ~100 Hz (Figure 4B). Thus, clustering alone cannot account for the complete loss of Brownian relaxation seen in Figure 4A, although the shift in the χ'' peak to lower frequency compared to the same particles in cell culture media (Figure 2C), reveals an increase in

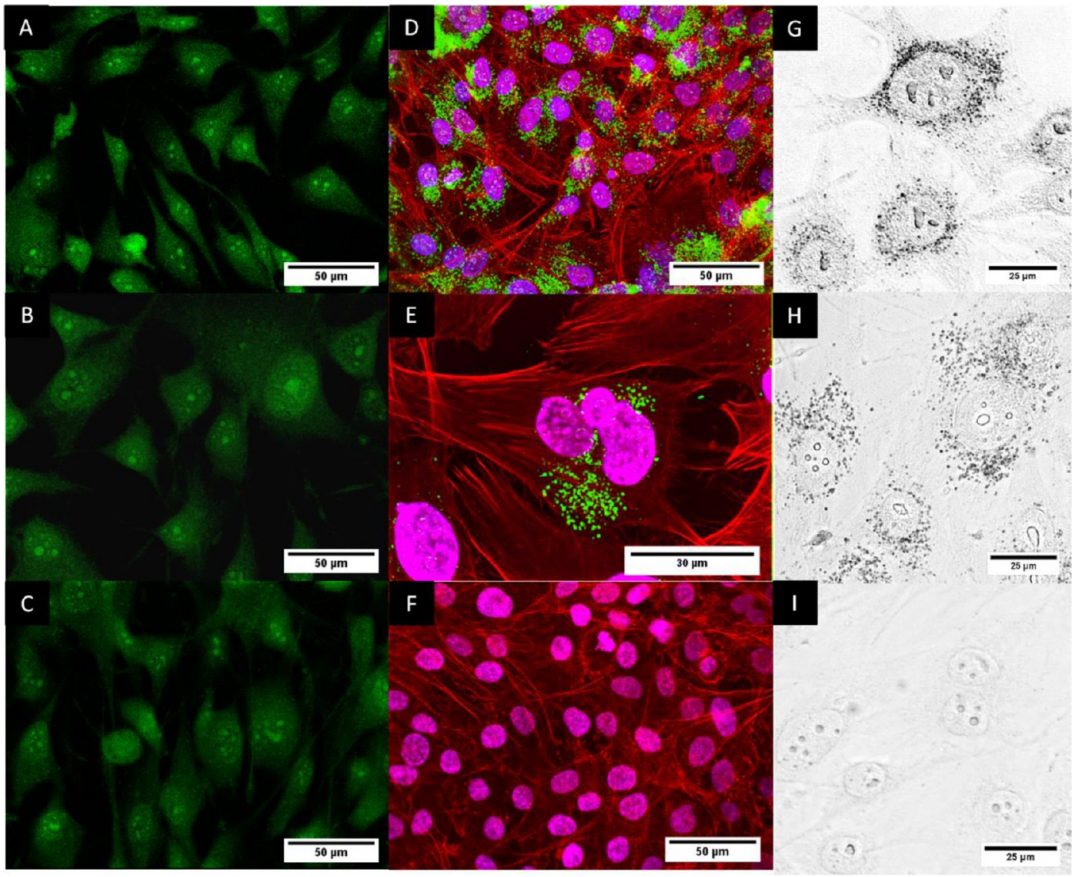

Figure 3. (A–C) Micrographs using fluorescence microscopy of human osteoblast-like MG-63 cells on glass cover slides stained with live/dead viability/cytotoxicity dyes (green-fluorescent calcein-AM stains for live cells and red-fluorescent ethidium homodimer-1 to indicate dead cells), following internalization of magnetically blocked nanoparticles (A), superparamagnetic nanoparticles (B), with control cells (particle free) shown in (C). Images were obtained after AC susceptibility measurements. Live cells are stained green and no dead cells (stained red) can be observed. (D–F) Composite confocal micrographs of vertical sections from the apex to the base of human osteoblast-like MG-63 cells using fluorescence and bright field microscopy. Morphology of cells cultured on glass cover slides with internalized magnetically blocked nanoparticles (D), superparamagnetic nanoparticles (E) and control cells (F). Cells were stained with ActinRed and Hoechst #33342. (G–I) Bright-field micrographs of the cells, following internalization of magnetically blocked nanoparticles (G), superparamagnetic nanoparticles (H), with control cells (particle free) shown in (I). Nanoparticles appear as black granules in the Bright-field images.

hydrodynamic size from ~127 nm in media to ~206 nm after the particles are released from cells.

Following sonication of lysed cells, the released magnetically blocked nanoparticles were restored almost to their original water suspension sizes (Figure 4C), with a measured peak in χ'' between that found for the same particles in media (Figure 2C) and water (Figure 2A). The hydrodynamic size of the sonicated particles (~76 nm) was significantly reduced from that found for the same particles after cell lysis (~206 nm), indicating that any clusters formed as result of cellular internalization could be easily broken down. Further, it was found that after sonication the nanoparticles retrieved from the cells could form stable suspensions in water, implying the preservation of the negatively charged citric acid coating originally used to create aqueous suspensions.

The interpretation of the AC susceptibility results was confirmed by transmission electron microscopy (TEM) of both the magnetically blocked and superparamagnetic nanoparticles obtained from particle suspensions in water, media and after cell lysis (Figure 5). While the formation of nanoparticle clusters can be seen in all cases, a thick surface coating due to the protein corona is only obvious in the nanoparticles obtained from the media suspensions (Figure 5B,E). In particular, the surface morphology of nanoparticle clusters in the original water suspensions (Figure 5A,D) and after cell lysis (Figure 5C,F) appears very similar, but with larger clusters formed in the latter case.

Significantly, the lack of the surface corona on nanoparticles after being released from the cells implies that the cells remove the particle protein coating before they store them. Although significant work has been done on the acute toxicity of iron oxide nanoparticles,[29,30] little is known about the degradation of iron oxide nanoparticles inside living cells.[31] In such cases the nanoparticles are exposed to various microenvironments as the cells interact with the nanoparticles; for example, they transfer them in

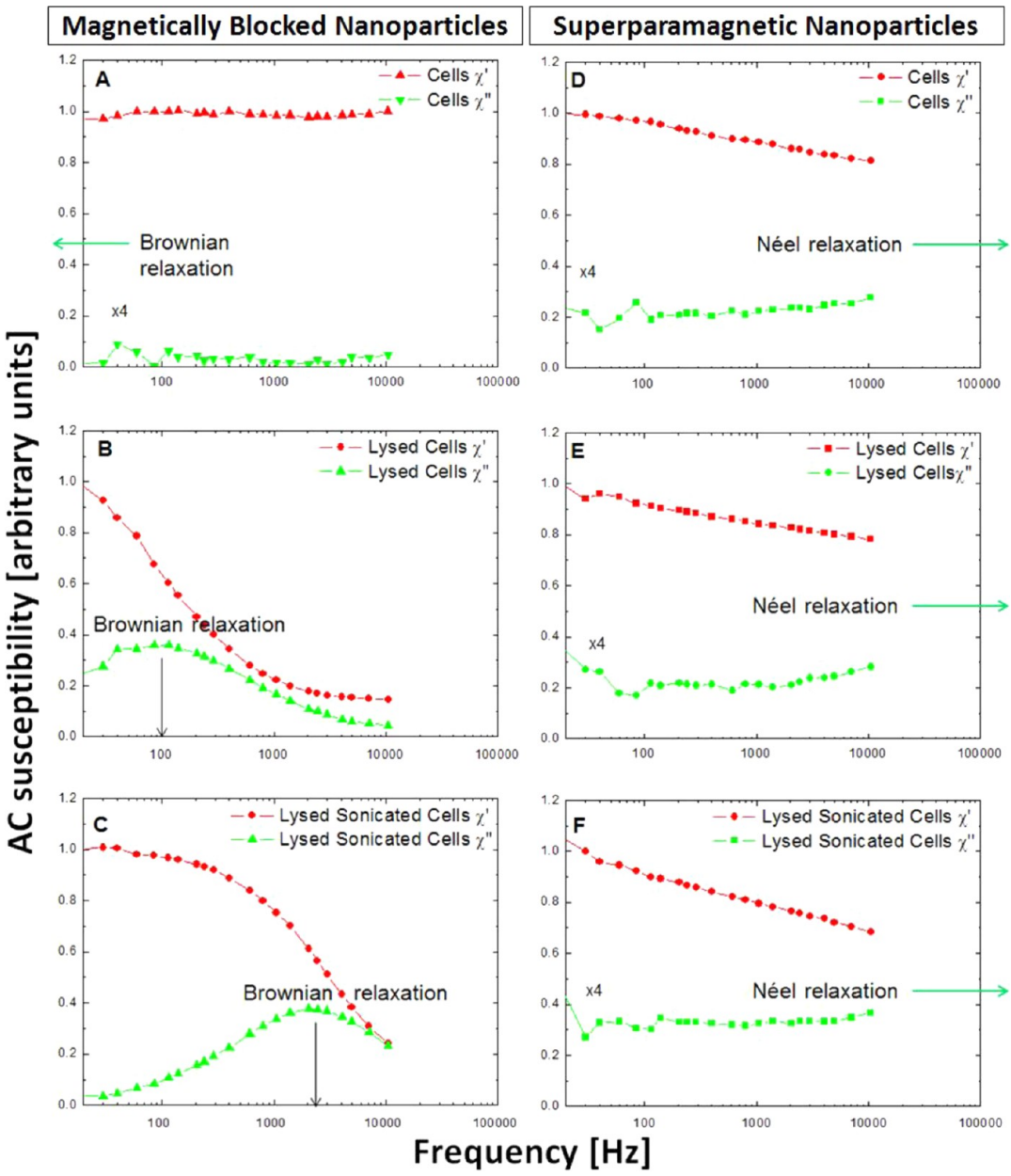

Figure 4. AC Susceptibility curves of live MG-63 cells with internalized magnetically blocked nanoparticles (A), freeze−thaw lysed cells with internalized nanoparticles (B) and the same freeze−thaw lysed cell sample following sonication for 60 min (C). (D−F) show the equivalent live MG-63 cell samples but with internalized superparamagnetic nanoparticles. χ'' signal is scaled ($\times$4) for samples where indicated. For ease of visualization, data were normalized such that the maximum χ' values were unity in each case. For more dilute samples (A−F) the frequency range was limited to 10 kHz because of the reduced sensitivity of the instrument at the higher frequencies.

lysosomes, which are highly specialized intracellular enzyme-containing organelles tasked with degrading material which is unessential for cell maintenance.[32] Thus, nanoparticles are exposed to dramatic changes in pH as they move from the extracellular microenvironment (pH 7.4), to the intracellular microenvironment (pH 6) and finally to lysosomes (pH 4.5).[33,34] Cells use an arsenal of digestive enzymes in this acidic environment to degrade the material, but also iron chelating agents[35] since iron is a biogenic element and iron homeostasis must be maintained.[36] Such processes could be responsible for the removal of the protein corona in the particles studied here, and also for the observed clustering effect. More generally, knowledge of the integrity of both the magnetic particle core and surface coatings, after cellular internalization, is important as these affect the nanoparticle properties both *in vitro* and *in vivo*.

Although TEM revealed that the smaller superparamagnetic nanoparticles underwent similar conformational changes to their larger magnetically blocked counterparts in the different microenvironments examined (Figure 5), the AC susceptibility curves obtained for these particles did not change

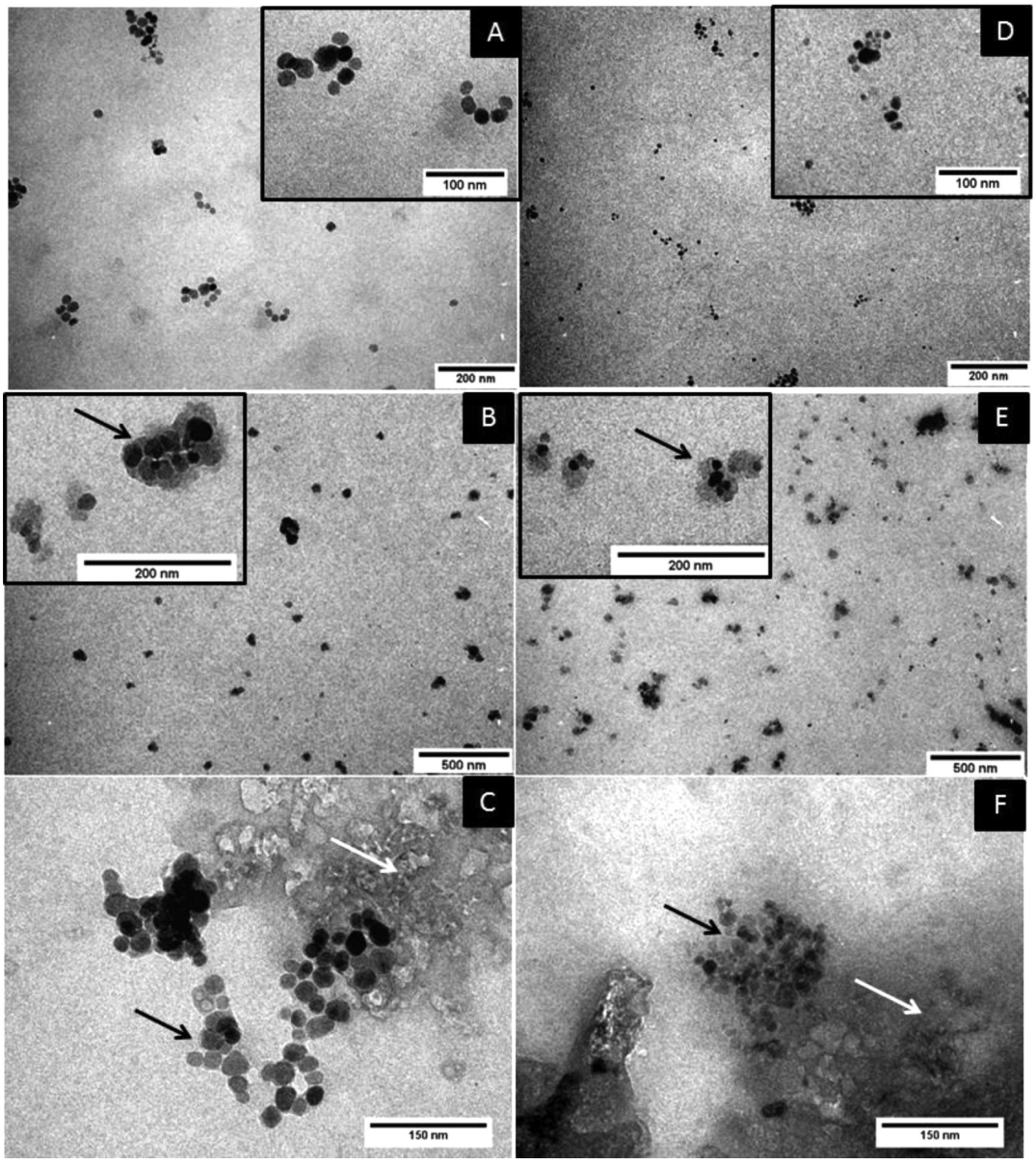

Figure 5. TEM micrographs of magnetically blocked nanoparticles in water (A) in cell culture media (B), arrow indicates the protein corona around the particle, and in freeze−thaw lysed MG-63 cells (C), black arrow indicates nanoparticles release without protein corona, white arrow shows cell debris. Superparamagnetic nanoparticles in water (D) cell culture media with the protein corona (black arrow) (E) and in freeze−thaw lysed MG-63 cells (F); black arrow indicates nanoparticles release without protein corona, white arrow shows cell debris.

(Figure 4D−F). This demonstrates the insensitivity of the Néel relaxation mechanism to the local microenvironment for the superparamagnetic nanoparticles, in contrast to the effects seen for Brownian relaxation of the magnetically blocked nanoparticles (Figure 4A−C). The fact that superparamagnetic nanoparticles undergo Néel relaxation in live cells is vital for intracellular hyperthermia, as suitably sized particles could generate heat by both magnetization relaxation and hysteresis losses. Conversely, the magnetically blocked nanoparticles used in this study were found to be immobilized inside live cells and so could not generate heat by relaxation processes. The intrinsic magnetic properties of such blocked magnetite nanoparticles also make them unsuitable for hysteresis heating, due to the limitations in AMF strength that can be safely applied in clinically based hyperthermia treatments.[37]

CONCLUSIONS

A novel application of AC susceptometry was used to probe the magnetization relaxation mechanisms of nanoparticles following internalization in live cells. The results presented demonstrate that the biological microenvironment significantly influences the magnetic response of nanoparticles, and can suppress Brownian relaxation for magnetically blocked nanoparticles in cells. However, the AC susceptibility signal corresponding to Néel relaxation in the superparamagnetic

nanoparticles was unaffected by changes to their biological microenvironement, emphasizing the importance of such intrinsic magnetic properties for hyperthermia applications when particle mobility cannot be guaranteed.[13] These results are in good agreement with recent studies that have shown that magnetic nanoparticles are immobilized in cancer cells but also when they are bound to the cell membrane.[38,39] This immobilization effect in turn caused a significant decrease in the heating capacity of magnetic nanoparticles *in vivo*.[38] Thus, magnetic nanoparticles that can generate heat solely through Brownian relaxation may be unsuitable for magnetic hyperthermia.[40]

The protein corona that developed on the nanoparticle surfaces after suspension in cell culture media appeared to be removed during cellular internalization. However, the integrity of the magnetic core and stabilizing citric acid coating were preserved, leading to the restoration of Brownian relaxation following the release of the particles by cell lysis. Thus, it seems that such nanoparticles have the potential to be recycled in usable form after cellular degradation, the implications of which must be considered for *in vivo* applications of magnetic nanoparticles. This key result raises the possibility that after hyperthermia treatment, the cancer cells will degrade (undergo apoptosis or necrosis) and the particles will be released by these degrading cells with their integrity maintained. The magnetic nanoparticles can then be reinternalized by cells previously unaffected by magnetic hyperthermia treatment which lays the basis for a repetition of the therapeutic procedure. Cells which reinternalize sufficient nanoparticles can be easily tracked with MRI, allowing *in vivo* localization of metastasised cells and future focused hyperthermia treatment.

The experiments reported here demonstrate the enormous potential for the application of AC Susceptometry techniques to probe the magnetic response of particles *in situ*. While relatively simple nanoparticle types representative of both blocked and superparamagnetic particles were chosen for this study, the same techniques could easily be used to explore a host of different particle types, coating materials and cellular structures, and could be extended to *ex vivo* and possibly *in vivo* studies. AC susceptibility also offers the possibility of real life monitoring of magnetic changes which could shed more light on cell−nanoparticle interactions in a time dependent manner, and could be used to noninvasively assess qualitative and quantitative cellular uptake of magnetic nanoparticles.[41]

As AC susceptibility measures only the response from a magnetic material it can be used on very complex matrices containing nonmagnetic material. Interestingly, the protein corona that developed on the particles in our experiments could act as a transient delivery system[42] to enhance biocompatibility and cellular uptake.[43] AC susceptibility could also prove effective to assess other delivery systems such as liposomes containing magnetic particles,[44,45] where a loss of Brownian relaxation could be used to detect the *in situ* breakdown of the liposome.

Finally, susceptibility measurements could also provide a useful insight into magnetic particle−particle interactions which could become significant where intracellular localization leads to the storage of particles in much more concentrated form. To date, it is not clear how such particle−particle interactions will affect the magnetic hyperthermia response, although some recent studies have suggested these effects could reduce the heating response of the particles.[46−48] It is thus important to determine whether particle−particle interactions occur *in vitro* and *in vivo*, and if necessary to assess the elimination of such effects through optimization of nanoparticle design.

MATERIALS AND METHODS

Nanoparticle Preparation. Two types of magnetite nanoparticles were investigated; a commercially available synthetic nanopowder (magnetically blocked nanoparticles) (Sigma) and biogenic nanoparticles (superparamagnetic nanoparticles) prepared as previously described.[25,26,49] Both magnetically blocked and superparamagnetic nanoparticles underwent citric acid coating as previously described[50,51] in order to stabilize them in water suspensions.

Nanoparticle Characterization. The AC susceptibility of citric acid coated nanoparticles was measured with particles suspended in water; pure glycerol, and Dulbecco's Modified Eagle Minimum Essential Medium (DMEM) (Lonza) supplemented with 10% fetal bovine serum (FBS) (HyClone) and 1% Penicillin and Streptomycin of 5000 U (Lonza). Measurements were performed using a home-built AC susceptometer operating within the frequency range 10 Hz−100 kHz at 37 °C. For more dilute samples (containing < 20 μg of magnetic material) the frequency range was limited to 10 kHz due to the reduced sensitivity of the instrument at the higher frequencies. The AC susceptibility curves were obtained by subtracting an appropriate background (*e.g.*, water, media or cells with no particles). A known mass of dysprosium oxide was used for calibration.

Particle hydrodynamic sizes were calculated from the AC susceptibility Brownian peaks based on the equation for the Brownian relaxation time

$$\tau_B = \frac{3\eta V_H}{k_B T} \quad (1)$$

Where V_H is the hydrodynamic volume of the particle, η is the dynamic viscosity of the fluid, k_B is Boltzmann's constant, and T is the absolute temperature. Particle hydrodynamic sizes in water were also determined using dynamic light scattering (Malvern Zetasizer 3000 HSA).

For TEM studies, a dilute drop of the sample was placed on a standard Formvar copper grid and left to air-dry. Once dry, TEM photomicrographs were obtained for nanoparticles both in media, and after the cell lysis, using a JOEL1230 TEM operating at 106 kV.

Cell Culture Experiments. For all cell culture experiments, T75 flasks (Corning) were seeded with osterosacroma-derived MG-63 cell line (passages 24−27). Each flask contained 1.5 million cells (approximately 20 000 cells/cm^2) and 10 mL of DMEM supplemented with 10% FBS and 1% penicillin and streptomycin. The cells were incubated at 37 °C in an air atmosphere with 5% of CO_2. On day 1 after seeding, cells were adherent to the flask and magnetic nanoparticle (MNP) suspensions were added into the media so that the final concentration of the nanoparticles was 100 μg/mL. The cells were cultured with MNPs for 3 days and on day 4 after seeding flasks were rinsed 3 times with PBS (Sigma) to remove all noninternalized nanoparticles. Cells were subsequently trypsinized (Lonza) in order to detach them and were thoroughly washed with and kept in media.

AC susceptibility was performed on cell suspensions in cell culture media for each nanoparticle type following internalization in live cells using the incubation procedure described above. One tenth of the cells with internalized nanoparticles were reseeded immediately after the AC susceptibility measurements onto glass cover slides in 24-well plate (Corning). 12 h after reseeding, the samples were divided into 2 groups. In the Group 1 cell viability was determined by the epifluorescence staining method, using the live/dead kit (Invitrogen). In the Group 2 the cells were fixed with 70% cold ethanol (4 °C) and stained with ActinRed (Molecular Probes) (Actin filament staining) and Hoechst #33342 (Invitrogen) (Nuclear staining). Photomicrographs of vertical sections from the apex to the base of human osteoblast-like MG-63 with a 200 nm step were taken using an Olympus FluoView FV 1200 confocal microscope.

Cells that were not reseeded were subjected to repeated freeze−thaw treatments and AC susceptibility was carried out on these lysed cells. The freeze−thaw lysed samples were subsequently sonicated for 60 min and repeat AC susceptibility measurements performed.

Image Processing. The contrast of the photomicrographs was enhanced by either ImageJ or Adobe Photoshop. Bright Field photomicrographs for the confocal composite image underwent several adjustments. First, contrast was enhanced, then the colors were inverted, further contrast adjustment was used when needed. In this case the particles appeared as white-colored granules on black background. Next, in order for the particles to appear as shown in the micrographs, their color was changed to bright green.

Conflict of Interest: The authors declare no competing financial interest.

Acknowledgment. The authors would like to thank J. Byrne, University of Tuebingen, for the preparation of the biogenic nanoparticles, J. Price for his assistance with confocal imaging, K. Walker for assistance with TEM and A. Black for fruitful discussions and generous advice. D. Soukup is supported by the European Commission under the FP7 Marie Curie Initial Training Network, "MagneticFUN". S. Moise is supported by the EPSRC Centre for Innovative Manufacturing in Regenerative Medicine (EP/H028277/1).

Supporting Information Available: Magnetic nanoparticle core size distributions determined from TEM analysis; calculated AC susceptibility from superparamagnetic nanoparticles; time dependent cellular uptake of biogenic magnetite nanoparticles measured by AC susceptibility. This material is available free of charge *via* the Internet at http://pubs.acs.org.

REFERENCES AND NOTES

1. Pankhurst, Q. A.; Thanh, N. T. K.; Jones, S. K.; Dobson, J. Progress in Applications of Magnetic Nanoparticles in Biomedicine. *J. Phys. D: Appl. Phys.* **2009**, *42*, 224001.
2. Zhang, E.; Kircher, M. F.; Koch, M.; Eliasson, L.; Goldberg, S. N.; Renström, E. Dynamic Magnetic Fields Remote-Control Apoptosis *via* Nanoparticle Rotation. *ACS Nano* **2014**, *8*, 3192–3201.
3. Muckle, D. S.; Dickson, J. A. Selective Inhibitory Effect of Hyperthermia on Metabolism and Growth of Malignant Cells. *Br. J. Cancer* **1971**, *25*, 771–778.
4. Jordan, A.; Scholz, R.; Wust, P.; Schirra, H.; Schiestel, T.; Schmidt, H.; Felix, R. Endocytosis of Dextran and Silan-Coated Magnetite Nanoparticles and the Effect of Intracellular Hyperthermia on Human Mammary Carcinoma Cells *in Vitro*. *J. Magn. Magn. Mater.* **1999**, *194*, 185–196.
5. Hilger, I.; Hiergeist, R.; Hergt, R.; Winnefeld, K.; Schubert, H.; Kaiser, W. A. Thermal Ablation of Tumors Using Magnetic Nanoparticles—an *in Vivo* Feasibility Study. *Invest. Radiol.* **2002**, *37*, 580–586.
6. Kettering, M.; Winter, J.; Zeisberger, M.; Bremer-Streck, S.; Oehring, H.; Bergemann, C.; Alexiou, C.; Hergt, R.; Halbhuber, K. J.; Kaiser, W. A.; *et al.* Magnetic Nanoparticles as Bimodal Tools in Magnetically Induced Labelling and Magnetic Heating of Tumour Cells: An *in Vitro* Study. *Nanotechnology* **2007**, *18*, 175101.
7. Hergt, R.; Dutz, S.; Roder, M. Effects of Size Distribution on Hysteresis Losses of Magnetic Nanoparticles for Hyperthermia. *J. Phys.: Condens. Matter* **2008**, *20*, 385214.
8. Chen, B. C.; Ho, C. Y.; Kao, L. J.; Wu, W. C.; Tsai, Y. H.; Ma, C. Hysteresis Loss-Induced Temperature in Ferromagnetic Nanoparticle. *IEEE Trans. Magn.* **2014**, *50*, 1000604.
9. Rosensweig, R. E. Heating Magnetic Fluid with Alternating Magnetic Field. *J. Magn. Magn. Mater.* **2002**, *252*, 370–374.
10. Glockl, G.; Hergt, R.; Zeisberger, M.; Dutz, S.; Nagel, S.; Weitschies, W. The Effect of Field Parameters, Nanoparticle Properties and Immobilization on the Specific Heating Power in Magnetic Particle Hyperthermia. *J. Phys.: Condens. Matter* **2006**, *18*, S2935–S2949.
11. Shliomis, M. I. Magnetic Fluids. *Phys.-Usp.* **1974**, *17*, 153.
12. Glöckl, G.; Hergt, R.; Zeisberger, M.; Dutz, S.; Nagel, S.; Weitschies, W. The Effect of Field Parameters, Nanoparticle Properties and Immobilization on the Specific Heating Power in Magnetic Particle Hyperthermia. *J. Phys.: Condens. Matter* **2006**, *18*, S2935.
13. Jeun, M.; Kim, Y. J.; Park, K. H.; Paek, S. H.; Bae, S. Physical Contribution of Neel and Brown Relaxation to Interpreting Intracellular Hyperthermia Characteristics Using Superparamagnetic Nanofluids. *J. Nanosci. Nanotechnol.* **2013**, *13*, 5719–5725.
14. Jordan, A.; Scholz, R.; Wust, P.; Fahling, H.; Felix, R. Magnetic Fluid Hyperthermia (MFH): Cancer Treatment with AC Magnetic Field Induced Excitation of Biocompatible Superparamagnetic Nanoparticles. *J. Magn. Magn. Mater.* **1999**, *201*, 413–419.
15. Fortin, J. P.; Wilhelm, C.; Servais, J.; Menager, C.; Bacri, J. C.; Gazeau, F. Size-Sorted Anionic Iron Oxide Nanomagnets as Colloidal Mediators for Magnetic Hyperthermia. *J. Am. Chem. Soc.* **2007**, *129*, 2628–2635.
16. Nutting, J.; Antony, J.; Meyer, D.; Sharma, A.; Qiang, Y. The Effect of Particle Size Distribution on the Usage of the AC Susceptibility in Biosensors. *J. Appl. Phys.* **2006**, *99*, 08B319.
17. Huang, C. Y.; Chen, P. J.; Ger, T. R.; Hu, K. H.; Peng, Y. H.; Fu, P. W.; Chen, J. Y.; Wei, Z. H. Optimization of Magnetic Labeling Process for Intracellular Hyperthermia in Cervical Cancer Cells. *IEEE Trans. Magn.* **2014**, *50*, 4003204.
18. Wilhelm, C.; Fortin, J. P.; Gazeau, F. Tumour Cell Toxicity of Intracellular Hyperthermia Mediated by Magnetic Nanoparticles. *J. Nanosci. Nanotechnol.* **2007**, *7*, 2933–2937.
19. Dong, J.; Zink, J. I. Taking the Temperature of the Interiors of Magnetically Heated Nanoparticles. *ACS Nano* **2014**, *8*, 5199–5207.
20. Chung, S. H.; Hoffmann, A.; Bader, S. D.; Liu, C.; Kay, B.; Makowski, L.; Chen, L. Biological Sensors Based on Brownian Relaxation of Magnetic Nanoparticles. *Appl. Phys. Lett.* **2004**, *85*, 2971–2973.
21. Ludwig, F.; Guillaume, A.; Schilling, M.; Frickel, N.; Schmidt, A. M. Determination of Core and Hydrodynamic Size Distributions of $CoFe_2O_4$ Nanoparticle Suspensions Using AC Susceptibility Measurements. *J. Appl. Phys.* **2010**, *108*, 033918.
22. Ferguson, R. M.; Khandhar, A. P.; Jonasson, C.; Blomgren, J.; Johansson, C.; Krishnan, K. M. Size-Dependent Relaxation Properties of Monodisperse Magnetite Nanoparticles

Measured over Seven Decades of Frequency by AC Susceptometry. *IEEE Trans. Magn.* **2013**, *49*, 3441–3444.
23. Bakoglidis, K. D.; Simeonidis, K.; Sakellari, D.; Stefanou, G.; Angelakeris, M. Size-Dependent Mechanisms in AC Magnetic Hyperthermia Response of Iron-Oxide Nanoparticles. *IEEE Trans. Magn.* **2012**, *48*, 1320–1323.
24. Muller, R.; Hergt, R.; Zeisberger, M.; Gawalek, W. Preparation of Magnetic Nanoparticles with Large Specific Loss Power for Heating Applications. *J. Magn. Magn. Mater.* **2005**, *289*, 13–16.
25. Byrne, J. M.; Telling, N. D.; Coker, V. S.; Pattrick, R. A. D.; van der Laan, G.; Arenholz, E.; Tuna, F.; Lloyd, J. R. Control of Nanoparticle Size, Reactivity and Magnetic Properties During the Bioproduction of Magnetite by Geobacter Sulfurreducens. *Nanotechnology* **2011**, *22*, 455709.
26. Byrne, J. M.; Coker, V. S.; Cespedes, E.; Wincott, P. L.; Vaughan, D. J.; Pattrick, R. A. D.; van der Laan, G.; Arenholz, E.; Tuna, F.; Bencsik, M.; *et al.* Biosynthesis of Zinc Substituted Magnetite Nanoparticles with Enhanced Magnetic Properties. *Adv. Funct. Mater.* **2014**, *24*, 2518–2529.
27. Safi, M.; Courtois, J.; Seigneuret, M.; Conjeaud, H.; Berret, J. F. The Effects of Aggregation and Protein Corona on the Cellular Internalization of Iron Oxide Nanoparticles. *Biomaterials* **2011**, *32*, 9353–9363.
28. Céspedes, E.; Byrne, J. M.; Farrow, N.; Moise, S.; Coker, V. S.; Bencsik, M.; Lloyd, J. R.; Telling, N. D. Bacterially Synthesized Ferrite Nanoparticles for Magnetic Hyperthermia Applications. *Nanoscale* **2014**, *6*, 12958–12970.
29. Weissleder, R.; Stark, D. D.; Engelstad, B. L.; Bacon, B. R.; Compton, C. C.; White, D. L.; Jacobs, P.; Lewis, J. Superparamagnetic Iron Oxide: Pharmacokinetics and Toxicity. *Am. J. Roentgenol.* **1989**, *152*, 167–173.
30. Chen, Z.; Yin, J.-J.; Zhou, Y.-T.; Zhang, Y.; Song, L.; Song, M.; Hu, S.; Gu, N. Dual Enzyme-Like Activities of Iron Oxide Nanoparticles and Their Implication for Diminishing Cytotoxicity. *ACS Nano* **2012**, *6*, 4001–4012.
31. Lévy, M.; Lagarde, F.; Maraloiu, V.-A.; Blanchin, M.-G.; Gendron, F.; Wilhelm, C.; Gazeau, F. Degradability of Superparamagnetic Nanoparticles in a Model of Intracellular Environment: Follow-up of Magnetic, Structural and Chemical Properties. *Nanotechnology* **2010**, *21*, 395103.
32. Arbab, A. S.; Wilson, L. B.; Ashari, P.; Jordan, E. K.; Lewis, B. K.; Frank, J. A. A Model of Lysosomal Metabolism of Dextran Coated Superparamagnetic Iron Oxide (SPIO) Nanoparticles: Implications for Cellular Magnetic Resonance Imaging. *NMR Biomed.* **2005**, *18*, 383–389.
33. Ohkuma, S.; Poole, B. Fluorescence Probe Measurement of the Intralysosomal Ph in Living Cells and the Perturbation of pH by Various Agents. *Proc. Natl. Acad. Sci. U. S. A.* **1978**, *75*, 3327–3331.
34. Ohkuma, S.; Moriyama, Y.; Takano, T. Identification and Characterization of a Proton Pump on Lysosomes by Fluorescein-Isothiocyanate-Dextran Fluorescence. *Proc. Natl. Acad. Sci. U. S. A.* **1982**, *79*, 2758–2762.
35. Kakhlon, O.; Cabantchik, Z. I. The Labile Iron Pool: Characterization, Measurement, and Participation in Cellular Processes. *Free Radical Biol. Med.* **2002**, *33*, 1037–1046.
36. Crichton, R. R.; Wilmet, S.; Legssyer, R.; Ward, R. J. Molecular and Cellular Mechanisms of Iron Homeostasis and Toxicity in Mammalian Cells. *J. Inorg. Biochem.* **2002**, *91*, 9–18.
37. Brezovich, I. A. Low Frequency Hyperthermia: Capacitive and Ferromagnetic Thermoseed Methods. *Med. Phys. Monogr.* **1988**, *16*, 82–111.
38. Di Corato, R.; Espinosa, A.; Lartigue, L.; Tharaud, M.; Chat, S.; Pellegrino, T.; Menager, C.; Gazeau, F.; Wilhelm, C. Magnetic Hyperthermia Efficiency in the Cellular Environment for Different Nanoparticle Designs. *Biomaterials* **2014**, *35*, 6400–6411.
39. Dutz, S.; Kettering, M.; Hilger, I.; Muller, R.; Zeisberger, M. Magnetic Multicore Nanoparticles for Hyperthermia-Influence of Particle Immobilization in Tumour Tissue on Magnetic Properties. *Nanotechnology* **2011**, *22*, 265102.
40. Dutz, S.; Hergt, R. Magnetic Nanoparticle Heating and Heat Transfer on a Microscale: Basic Principles, Realities and Physical Limitations of Hyperthermia for Tumour Therapy. *Int. J. Hyperthermia* **2013**, *29*, 790–800.
41. Zysler, R. D.; Lima, E.; Mansilla, M. V.; Troiani, H. E.; Pisciotti, M. L. M.; Gurman, P.; Lamagna, A.; Colombo, L. A New Quantitative Method to Determine the Uptake of Spions in Animal Tissue and Its Application to Determine the Quantity of Nanoparticles in the Liver and Lung of Balb-C Mice Exposed to the Spions. *J. Biomed. Nanotechnol.* **2013**, *9*, 142–145.
42. Ding, H. M.; Ma, Y. Q. Computer Simulation of the Role of Protein Corona in Cellular Delivery of Nanoparticles. *Biomaterials* **2014**, *35*, 8703–8710.
43. Calatayud, M. P.; Sanz, B.; Raffa, V.; Riggio, C.; Ibarra, M. R.; Goya, G. F. The Effect of Surface Charge of Functionalized Fe_3O_4 Nanoparticles on Protein Adsorption and Cell Uptake. *Biomaterials* **2014**, *35*, 6389–6399.
44. Kong, G.; Braun, R. D.; Dewhirst, M. W. Hyperthermia Enables Tumor-Specific Nanoparticle Delivery: Effect of Particle Size. *Cancer Res.* **2000**, *60*, 4440–4445.
45. Needham, D.; Anyarambhatla, G.; Kong, G.; Dewhirst, M. W. A New Temperature-Sensitive Liposome for Use with Mild Hyperthermia: Characterization and Testing in a Human Tumor Xenograft Model. *Cancer Res.* **2000**, *60*, 1197–1201.
46. Branquinho, L. C.; Carriao, M. S.; Costa, A. S.; Zufelato, N.; Sousa, M. H.; Miotto, R.; Ivkov, R.; Bakuzis, A. F. Effect of Magnetic Dipolar Interactions on Nanoparticle Heating Efficiency: Implications for Cancer Hyperthermia. *Sci. Rep.* **2013**, *3*, 2887.
47. Lima, E.; Vargas, J. M.; Rechenberg, H. R.; Zysler, R. D. Interparticle Interactions Effects on the Magnetic Order in Surface of Fe_3O_4 Nanoparticles. *J. Nanosci. Nanotechnol.* **2008**, *8*, 5913–5920.
48. Morup, S.; Hansen, M. F.; Frandsen, C. Magnetic Interactions between Nanoparticles. *Beilstein J. Nanotechnol.* **2010**, *1*, 182–190.
49. Byrne, J. M.; Coker, V. S.; Moise, S.; Wincott, P. L.; Vaughan, D. J.; Tuna, F.; Arenholz, E.; van der Laan, G.; Pattrick, R. A. D.; Lloyd, J. R.; *et al.* Controlled Cobalt Doping in Biogenic Magnetite Nanoparticles. *J. R. Soc., Interface* **2013**, *10*, 20130134.
50. Racuciu, M.; Creanga, D. E.; Airinei, A. Citric-Acid-Coated Magnetite Nanoparticles for Biological Applications. *Eur. Phys. J. E: Soft Matter Biol. Phys.* **2006**, *21*, 117–121.
51. Coker, V. S.; Telling, N. D.; van der Laan, G.; Pattrick, R. A. D.; Pearce, C. I.; Arenholz, E.; Tuna, F.; Winpenny, R. E. P.; Lloyd, J. R. Harnessing the Extracellular Bacterial Production of Nanoscale Cobalt Ferrite with Exploitable Magnetic Properties. *ACS Nano* **2009**, *3*, 1922–1928.